Journal of Ovonic Research Vol. 12, No. 3, May- June 2016, p. 137 - 146

ELECTRIC MODULUS PROPERTIES OF PRASEODYMIUM SUBSTITUTED COPPER FERRITES

M. T. FARID, I. AHMAD*, G. MURTAZA, M. KANWAL, I. ALI
Department of Physics, Bahauddin Zakariya University Multan, 60800 Pakistan

A series of Praseodymium substituted spinel ferrites with nominal composition of $CuPr_yFe_{2-y}O_4$(y = 0.00, 0.02, 0.04, 0.06, 0.08, 0.10) were synthesized by the sol-gel technique. Temperature dependent DC electrical conductivity and drift mobility were found in good agreement with each other, reflecting semiconducting behavior. The presence of Debye peaks in imaginary electric modulus curves confirmed the existence of relaxation phenomena in given frequency range. The AC conductivity indicating that the mechanism is due to polaron hopping. In the present ferrite system, Cole–Cole plots were used to separate the grain and grain boundary effects. Substitution of Pr leads to a remarkable rise of grain boundary resistance as compared to the grain resistance. As both AC conductivity and Cole–Cole plots are the functions of concentration, they reveal the dominant contribution of grain boundaries in the conduction mechanism. Due to these remarkable characteristics, it is suggested that these synthesized materials are suitable for power applications and high frequency multilayer chip inductors.

(Received March 13, 2016; Accepted May 27, 2016)

Keywords: Spinel ferrites, DC conductivity, Grain boundaries, Conduction mechanism, Drift Mobility

1. Introduction

Spinel ferrites have attracted increasing attention due to their superior features, including reasonable cost, mechanical hardness, chemical stability at high temperature and high DC resistivity [1], extraordinary elasticity in tuning the magnetic properties and simplicity of synthesis [2]. These ferrites have the inordinate prospective to be the subsequent application of microwave absorption, satellite communication, memory devices, antennas cores, computer components, permanent magnets, magnetic sensors, ferrofluids, drug delivery, actuators, high-density storage, microwave absorbing materials, magnetic recording media, transformer cores, read/write heads ,hyperthermia for cancer treatment, magneto-caloric refrigeration, gas sensors and contrast enhancement in magnetic resonance imaging (MRI) [3-12]. It can be predicted that thin films of ferrite are the potential candidate for future of high-density recording due to excellent mechanical durability and low noise quality [14]. It has advantage, ferrites operates on the principle of high frequency requires low loss and low electrical conductivities [15] Ferrites nanoparticles are frequently used for microwave devices preparation [16, 17] due to remarkable small electrical conductivity and dielectric losses. The control of electrical conductivity in ferrites is a serious problem. The various techniques have been adopted to decrease the electrical conductivity by controlling the sintering temperature, reaction temperature, the concentration and type of impurities. Many researchers are trying to develop a light weight, integrating, tunable and multifunction devices on the biases of electrical properties in the field of nano-technology. Several research groups are studying copper as base material due to their interesting electrical, magnetic properties and crystal changes heat treatment [16-17]. In addition, copper ferrite is distinguished among other spinel ferrites by the fact that it undergoes a structural phase transition accompanied by a reduction in the crystal symmetry to tetragonal structure [16, 18].

* Corresponding author: ishtiaqahmad@bzu.edu.pk

Substitution of different cations in copper ferrite materials induces variations in electrical properties [13,14]. Among of them rare-earth ion substitution in ferrites has been reported by many researchers to enhance their electrical and magnetic properties [15–18].

An attempt is made in this paper to tailor the electrical parameters like DC electrical resistivity, dielectric constant, dielectric loss, dielectric tangent loss factor, AC conductivity of Pr^{3+} substituted Copper ferrites. The sol-gel auto combustion technique was employed for synthesis due to ease of handling, cost effective and is used to produce submicron sized particles with high degree of homogeneity and good control of stoichiometry [3].

2. Experimental

2.1 Sample Preparation

Sol-gel technique followed by auto-combustion was employed to synthesize the Nano crystalline ferrites of general formula $CuPr_yFe_{2-y}O4$ whereas the value of "y" ranged between 0 and 0.1 with the continuous intervals of 0.02. The stoichiometric amounts of $FeCl_3$, Cu $(NO_3)_2$ were dissolved in deionized water where as Pr_2O_3 (99.99% pure) was first dissolved in HNO_3 in order to obtain praseodymium nitrate and then mixed with the solution. The deionized water 100 ml was taken in a Pyrex beaker to initially dissolve the analytical grade Cu $(NO_3)_2$, Pr_2O_3 (99.99% pure) and $FeCl_3$. Citric acid was employed as a Chelating agent to obtain transparent and homogeneous solution. A temperature of 80 ^oC was used for the homogeneous mixing of dissolved solution in the magnetic stirrer. Ammonia solution was continuously added and stirred for almost seven hours to maintain the pH value at 7. The solution changed into a viscous gel on evaporation followed by self-combustion occurring at a temperature of 370 ^oC. When the dry gel was completely burnt, it transformed into a fluffy powder which was called "Precursor powder". The powder was then completely grinded, pre-sintered in a furnace at 700 ^oC for 5 hours and then annealed. At Paul–Otto Weber Hydraulic Press was used to apply a load of about 30 KN to press the sintered powder into pellets. 3-5% by weight polyvinyl alcohol was used to as a binder to form the pellets. The evaporation of binder was made for 1 hour at 250 ^oC followed by the sintering of samples for 7 hours at 950 ^oC.

2.2 Characterization

The DC electrical conductivity was measured by a simple two-probe method in the temperature range 300–573 K. A Keithly source meter model-197 was used for the said purpose. The Dc conductivity (σ_{DC}) was calculated using the following relation [19].

$$\sigma_{Dc} = \frac{d}{RA} \qquad (1)$$

Where "R" is resistance of the sample, "A" is area of the sample pellet and "d" is thickness of the sample pellet.

Drift mobility (μ_d) was calculated using relation [19].

$$\mu_d = \frac{\sigma_{Dc}}{ne} \qquad (2)$$

where "e" is charge of the electron, "σ_{DC}" is DC conductivity and "n" is the concentration of charge carrier which can be calculated from the well-known equation: [19]

$$n = \frac{N_A d_b P_{Fe}}{M} \qquad (3)$$

where N_A is the Avogadro's number, d_b is the measured bulk density of sample, P_{Fe} is the number of iron atoms in the chemical formula of ferrites and M is the molecular weight of the samples.

The AC conductivity was calculated from dielectric constant and dielectric loss tangent (tan δ) as

$$\sigma_{Ac} = 2\pi f \varepsilon_o \varepsilon' \tan\delta \qquad (4)$$

where "σ_{AC}" is the AC conductivity, "f" is the frequency, "ε_o" is the permittivity of free space and "ε'" is the real part of dielectric constant. The real and imaginary parts of the electrical modulus M' and M″ respectively can be calculated as follows [20]

$$M' = \frac{\varepsilon'}{(\varepsilon'^2 + \varepsilon''^2)} \qquad (5)$$

$$M'' = \frac{\varepsilon''}{(\varepsilon'^2 + \varepsilon''^2)} \qquad (6)$$

Where ε' and ε" is the real part of the dielectric constant and imaginary part of dielectric constant, respectively. Dielectric data and impedance were measured by using Agilent impedance analyzer model E4991ARF. Impedance measurements were performed in the frequency range from 1 MHz to 3 GHz at room temperature by taking the absolute value of impedance |Z| with varying complex angle θ_Z. The real and imaginary parts of impedance can be written as

$$Z' = R = |Z| \cos\theta_Z \qquad (7)$$

$$Z'' = X = |Z| Sin\theta_Z \qquad (8)$$

Where R and X are the real and imaginary parts of impedance, respectively.

3. Results and Discussions

3.1 DC electrical conductivity

Temperature dependent DC electrical conductivity of Pr substituted CuPryFe2-yO_4 spinel ferrites was measured by two-probe method in the temperature range of 293-677 K.

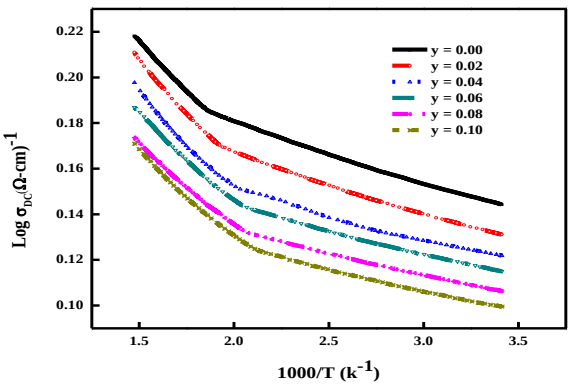

Fig. 1. Change in DC electrical conductivity with temperature for for $CuPr_yFe_{2-y}O_4$ ferrites.

Figure. 1 shows that the conductivity increases with the increase of temperature. This behavior is analogous of semiconductor behavior of the prepared samples. The increase in the drift

mobility of the charge carrying particles might be the reason for the increase of conductivity with the increase of temperature. The DC conductivity curve vs 1000/T shows two distinct areas. Many researchers also observed a similar kind of behavior [21-22]. The first area of the ferrites appears for low temperature. At high temperatures, the conductivity is increased. This happens due the initiation of hopping phenomenon of the charge carrying particles from one site to the other. There are low activation energies in the first region of the ferrites which suggest that the conduction of the region takes place by the free charge carrying particles. The appearance of the second region takes place at high temperatures and it is suggested that it is due to the polaron hopping at high activation energy. A good correspondence is shown by comparing the compositional dependence for activation energy and DC conductivity. The samples of low conductivity have high activation energy and vice versa [23-24]. The explanation for this decrease might be the cation distribution at different sites in spinel ferrites. The octahedral sites are occupied by Pr^{3+}ions whereas Fe and Cu ions occupy both A and B sites [25-26]. The conductivity of ferrites is dependent upon the hopping of electrons between Fe^{3+} and Fe^{2+} ions at A and B sites, respectively.

Since B site is occupied by Pr^{3+} ions, therefore the number of Fe ions at this site is decreased. This subsequently decreases the hopping of electrons between Fe^{2+} and Fe^{3+} ions. Ultimately, the conductivity is decreased.

3.2. Drift mobility

The drift mobility of $CuPr_yFe_{2-y}O_4$ spinel ferrites was calculated from the experimentally observed data of the electrical conductivity. The relationship of calculated drift mobility with temperature is given by the following equation [27].

$$\mu_d = \mu_o Exp[\frac{-E_\mu}{K_B T}] \qquad (9)$$

Here μ_o is the pre-exponential constant, k_B represents the Boltzmann constant and E_μ is the activation energy for mobility of ions.

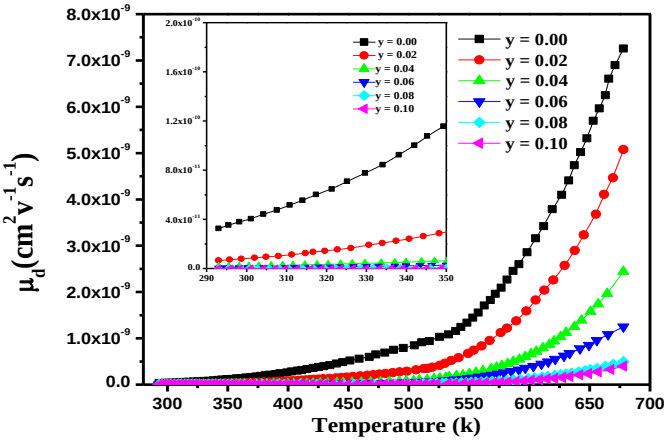

Fig. 2. Change in drift mobility with temperature for for $CuPr_yFe_{2-y}O_4$ ferrites.

The calculated data of charge carrier mobility strongly agree with the experimental data of electrical conductivity. It is clear from the figure 2 that charge carrier mobility value is maximum for $CuPr_yFe_{2-y}O_4$ (y = 0.00). All the samples have low values of drift mobility as compared to typical semiconductors. However, these results of mobility are not strange as far as spinel ferrite semiconductors are concerned; however such type of low values has been already presented by many researchers [28–31]. The graph between charge carrier mobility as a function of temperature is shown in figure 2. It is clear from this figure that with the increase of temperature, the drift mobility increases continuously. This behavior of drift mobility strongly suggests that the conduction mechanism in all these praseodymium substituted spinel ferrites is due to the hopping

of charge carrier electrons from Fe^{2+} to Fe^{3+} and holes transfer from Cu^{1+} to Cu^{2+}. Such types of results have been reported by several researchers [28–31].

3.3 AC conductivity

AC conductivity for $CuPr_yFe_{2-y}O_4$ spinel ferrites as a function of frequency (1 MHz to 3 GHz) is shown in figure 3.

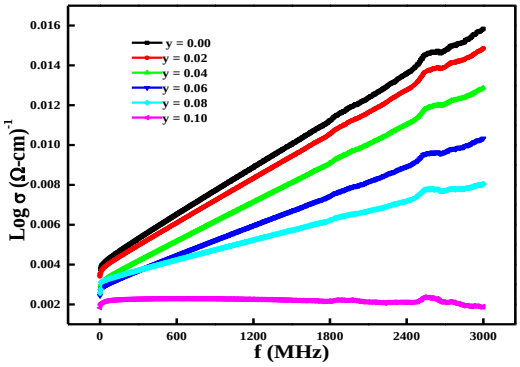

Fig. 3.Variation in AC conductivity with frequency for $CuPr_yFe_{2-y}O_4$ ferrites. at room temperature.

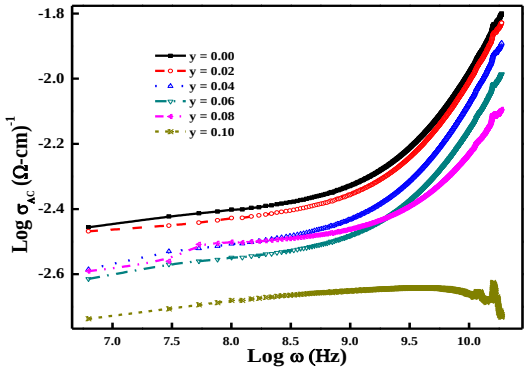

Fig. 4.Variation of AC conductivity with ln f for $CuPr_yFe_{2-y}O_4$ ferrites.

There is a linear increase in σ_{AC} with the applied AC field. The response of Ac conductivity with the applied AC field is presented by the relation.

$$\sigma_{tot}(\omega) = \sigma_{DC} + A\omega^n \qquad (10)$$

Here A is the pre-exponential factor having same units as that of DC conductivity, n represents the frequency exponent whose value is always less than one, while ω is the applied angular frequency. Fig. 4 represents the variation of log σ_{ac} with log ω of $CuPr_yFe_{2-y}O_4$ ferrites at room temperature in the frequency range of 1 MHz to 3 GHz was used. It is clear from the figure that all the samples show the gradual increase in the AC conductivity with the increase in frequency. This increase in AC conductivity is observed due to the increase in hopping frequency of the charge carriers between Fe^{2+} and Fe^{3+} ions on tetrahedral and octahedral sites. The Ac conductivity can be explained on the basis of Maxwell–Wagner's model. According to Koop's phenomenological theory and Maxwell–Wagner's model spinel ferrites are composed of conducting grains and grain boundaries. The resistive thin films separate the grain boundaries and the conducting grains from each other. In the low frequency region, grain boundary contribution is attributed to the variation

of ac conductivity because the hopping frequency between Fe^{3+} and Fe^{2+} is less which is also reported by [32, 33]. However, for high frequency values, the increasing polarization at adjacent sites and grain effect play important role to increase the conductivity [29, 30]. The substitution of Pr contents replaces the iron ions from octahedral site, so hopping between Fe^{2+} and Fe^{3+} ions decreases, hence the AC conductivity decreased. Similar results have also been reported by many researchers [31-32].

3.4 Impedance

The Impedance analysis is the best tool to understand the electrical properties of synthesized spinel ferrites. This method gives the data for resistive (real) and reactive (imaginary) part which contribute in conduction on the application of an A.C field [32]. The complex impedance plot is the best way to understand the contribution of microstructure (grains and grains boundary).The graph between impedance and frequency is shown in fig 5.

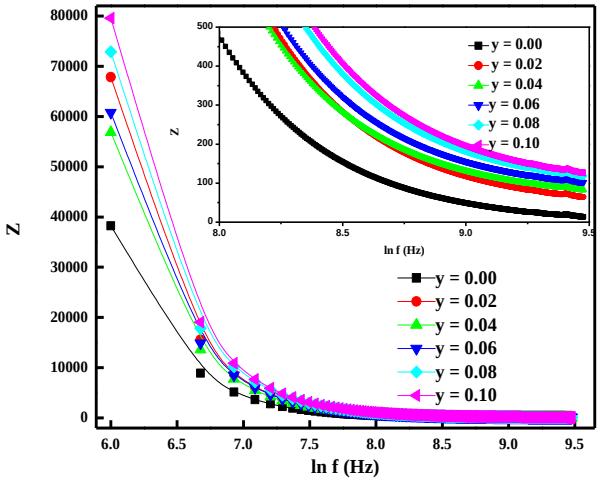

Fig. 5.Variation of Impedance with ln f of for $CuPr_yFe_{2-y}O_4$ ferrites.

It has been found that the values of impedance and its components increase with Pr substitution which is very much consistent with compositional dependence of AC conductivity, i.e. increase in impedance results in decrease in AC conductivity. It is found that the magnitude of Z decreases with the increase of frequency, indicating increase in AC conductivity. It also indicates the semiconducting type behavior in these samples. It is a well-known fact that cu^{1+} is oxidized to cu^{2+} during heat treatment and create positive holes. The operative mechanism of conductivity is subjected to the hopping of both electrons and positive holes.

3.5. Cole–Cole (or Nyquist) diagram

The relaxation phenomenon of the material is studied by using powerful techniques such as Complex impedance spectroscopy (CIS). Grains as well as grain boundaries which are the interaction between the particles are also studied by using this technique. Material electrode contribution, grain boundary and separate bulk (grains) can be easily separated by considering the electrical properties. The use of the imaginary part of conductance (Y'') and impedance (Z'') is suitable for conductive and resistive analysis under the dominance of long range conductivity. But the imaginary part of the electrical modulus (M'') and permittivity (ε'') are suitable under the dominance of localized relaxation. Polarization analysis provides the base to the Complex electric modulus formalism and the electrical behavior of ferroelectric samples can be analyzed by using the aforesaid formalism [34]. Complex electric modulus formalism plays an important role for inhomogeneous natured polycrystalline ceramics for which the complex impedance graphs don't distinguish between the bulk density effects and the grain boundary effects [35]. The impedance behavior of various materials is explained by Cole-Cole diagram. The complex parameters i.e.

Admittance, Impedance, dielectric loss, electric modulus and Permittivity can be employed to draw the Cole-Cole diagrams. The characteristics and behavior of these parameters are related to each other. The relationships are as follows:

$$\tan\sigma = \frac{\varepsilon''}{\varepsilon'} = \frac{Y''}{Y'} = \frac{Z''}{Z'} = \frac{M''}{M'}$$

The dielectric modulus' calculation helps to resolve the relaxation process. The relationships between imaginary and real components of dielectric are as under [36].

$$M' = \frac{\varepsilon'}{(\varepsilon'^2 + \varepsilon''^2)}$$

$$M'' = \frac{\varepsilon''}{(\varepsilon'^2 + \varepsilon''^2)}$$

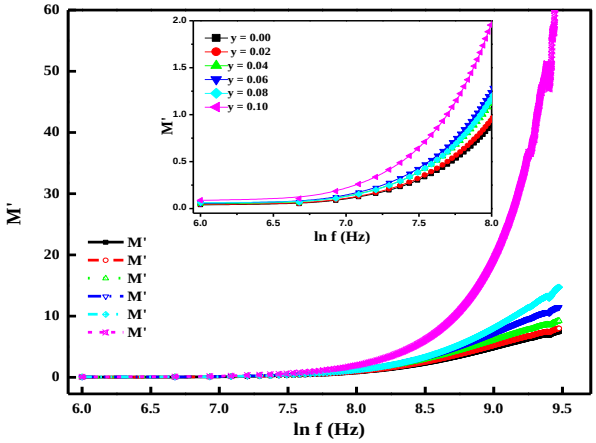

Fig. 6. Variation of complex electric modulus (real part M') with ln f

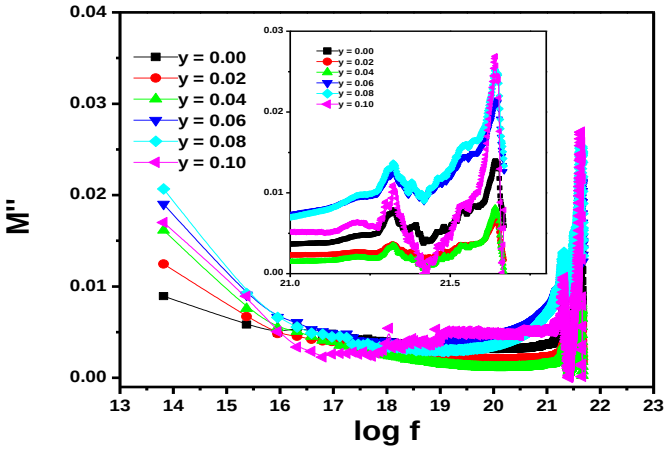

Fig. 7. Variation of complex electric modulus (imaginary part M'') with log f

Electric modulus is employed to analyze the dependency of frequency for the interfacial polarization effect of $CuPr_xFe_{2-x}O_4$ ferrites. Figure 6 and 7 shows the variation of Electric modulus (real and imaginary) as a function of frequency. The relaxation peaks are displaced by the

accumulation of electric charges around the ceramic particles. The fact of the matter is that if small volume is occupied by the continuity region of grain particles, the spectrum of impedance (Z'' vs Z') has better visualization for the plane's semi-circles. In case, a large volume is occupied by the grain boundaries' region, the plot between M' and M'' gives better understanding of semicircles [37]. The grain boundaries behavior's relationship and peaks' appearance confirmed the latter behavior. No peak appearance in the graphs of complex impedance and loss tangent confirmed the only peak appearance for imaginary electric modulus vs. frequency graphs as shown in fig. 7. Since the size of the Nano-ferrites is small, therefore the grain boundaries have high density. The lack of Fe ions and the irregular arrangement of atoms close to the grain boundaries might be the possible reasons for higher grain boundaries' values. The single semi-circle appearance from Cole-Cole graphs confirms the unique role of grain boundaries in the conduction process. Furthermore, M'' has an inverse relationship with capacitance, thus we observe the bulk effects in the complex modulus spectra. Moreover, the existence of relaxation times' distribution causes the peaks of spectra to appear.

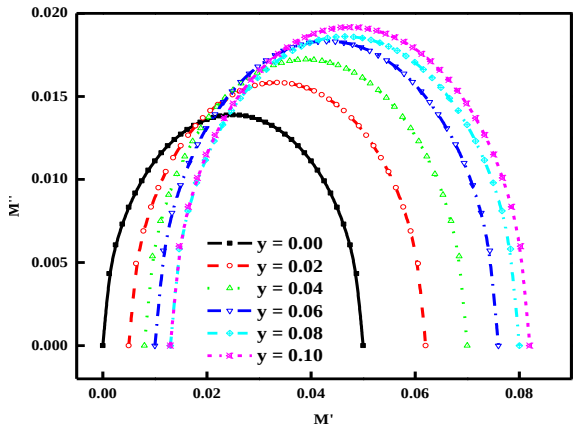

Fig. 8. Cole-Cole plots for $CuPr_yFe_{2-y}O_4$ ferrites.

The non-Debye natured curve's appearance and the peak's appearance in the spectra are due to the intrinsic dispersion of the materials [38, 39].

Fig. 8 shows that only one semi-circle appeared from all of the samples under study. Fig. 8 shows that the frequency of medium to high range was employed i.e. 1.3 GHz-3 GHz. However the semi-circle radius of various samples changed in accordance with Pr^{3+} substitution [40]. Jump relaxation model (JRM) also explains the observed spectra [41]. The model tells us that in the low frequency region the conduction takes place as a result of the hopping of Fe ions between A– and B–sites. But in the high frequency region, the hopping is restricted substantially. The frequency dispersion takes place due to the variation in the ratio of successful to unsuccessful hops with the increasing values of frequency. The JRM also elaborates that various activation energies are association with both unsuccessful and successful hopping processes [42].

3.6. Q values

Fig. 9 shows the variation in Q values with change in frequency for Pr substituted $CuPr_yFe_{2-y}O_4$ spinel ferrites.

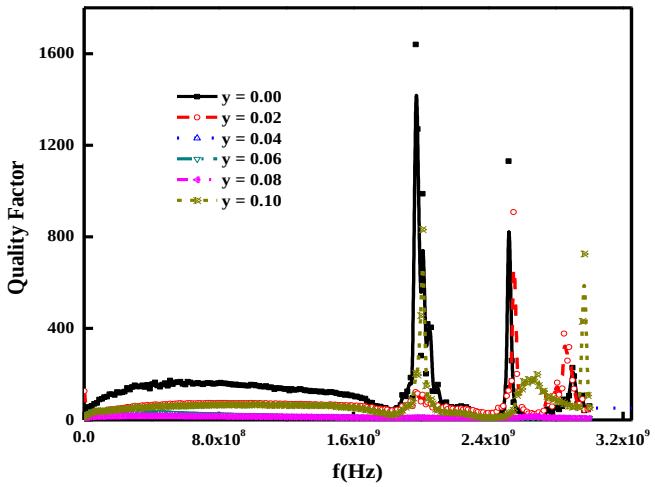

Fig. 9.Variation of Q values with frequency of Pr substituted $CuPr_yFe_{2-y}O_4$ ferrites.

It is observed that the values of quality factor (Q) are more at higher frequency regions. Thus high Q values and a resonance frequency above 2 GHz clearly suggest that these materials can be used in high frequency multilayer chip inductors [43].

4. Conclusions

The observed mechanism of conductivity is mainly due to the hopping of holes and electrons.

- DC electrical conductivity decreased due to the cations distribution at various sites in the spinel structure.
- AC conductivity at low frequency region describes the grain boundary behavior, while the dispersion at high frequency can be attributed to the conductivity of grains.
- The complex impedance plane plots showed a single semicircle, indicating the capacitive and resistive properties of the materials, due to contribution of grains and grain boundaries in the samples.
- Appreciable improved values of quality factor suggested the possible use of these synthesized material for power applications and high frequency multilayer chip inductors.

References

[1] I.H. Gul, I.H, W. Ahmed, A.Maqsood, J. Magn. Magn.Mater.**320**,270 (2008).
[2] M.A.Gabal and Y.M.A Angari, Materials Chemistry and Physics **118**, 153(2009).
[3] I.H. Gul and E. Pervaiz, Materials Research Bulletin **46**, 1353(2012).
[4] Y.M.Abbas, S.A.Mansour, M.H. Ibrahim, S.E.Ali, J. Magn. Magn.Mater.**23**, 2748(2011).
[5] A. Thakur, P. Thakur, J. H. Hsu, Journal of Applied Physics **111**, 07A305 (2012).
[6] S. Singhal, J. Singh, S.K. Barthwal, S.K., Chandra, K.: J Solid State Chem**178**, 3183 (2010).
[7] G. Murtaza, I. Ahmad, A. hakeem, P. Mao, X. Guohua, M. T. Farid, G. Mustafa, M. Kanwal, M. Hussain, M. Ahmad, J. Nanomaterials and Biostructures, **10**(4),1393-1401 (2015).
[8] D.R Mane, D.D. Birajdar, S. Patil, S.E. Shirsath, R.H. Kadam, J. of Sol-Gel Science and Technology **58**, 70(2010).
[9] M. Hashim, K. S. Alimuddin, S.E. Shirsath, R.K. Kotnala, J.Shah, R. Kumar, Materials Chemistry and Physics **139**, 364(2013).
[10] K.M. Batoo, S. Kumar, International J. of Nanoparticles **2**, 416(2009).

[11] S. Kubickova, J. Vejpravova, P. Holec, D.Niznansky, J. Magn. Magn.Mater. **334**,102 (2013).
[12] P.P. Hankare, K.R. Sanadi, K.M. Garadkar, D.R. Patil, I.S. Mulla, J. Alloys Comp **553**,383 (2013).
[13] I.H. Gul, A.Maqsood, J. Alloys Comp**465**, 227(2008).
[14] B.H. Ryu, H.J. Chang, Y.M. Choi, K.J. Kong, J.O. Lee, C.G.Kim, H.K. Jung, J.H. Byun, Phys. Stat. Sol. (a) **201**, 1855(2004).
[15] N. Rezlescu, E. Rezlescu, C. Pasnicu, M.L. Craus, J. Mang. Mang.Mater 136, 319 (1994).
[16] V. Sepelak, D. Baabe, F.J. Litterst, K.D. Becker, J. Appl. Phys 88, 5884 (2000).
[17] Martha Pardavi-Horvath, J. Mang. Mang.Mater**215**, 171 (2000).
[18] I. Ahmad, T. Abbas, M.U. Islam, A. Maqsood, Ceramics International**39**, 6735 (2013).
[19] H.O. Rodrigues, G.F.M. Pires Junior, A.J.M. Sales, P.M.O. Silva, B.F.O. Costa,Alcantara Jr, S.G.C. Moreira, A.S.B. Sombra, Physica B **406**, 2532 (2011).
[20] M.A. El Hiti, A.M. Abo El Ata, J. Magn. Magn.Mater**195**, 667 (1999).
[21] A.M. El-Sayed, Mater. Chem. Phys**82**, 583 (2003).
[22] M. Ishaque, M.U. Islam, I. Ali, M.A. Khan, I.Z. Rahman, Ceram. Int**38**, 3337 (2012).
[23] J. Smit, H.P.J. Wijn, Ferrites, Wiley, NY, USA, (1959).
[24] D. Kothari, V.R. Reddy, V.G. Sathe, A. Gupta, A. Banerjee, A.M. Awasthi, J. Magn.Magn. Mater**320**,548 (2008).
[25] M.A. Iqbal, M.U. Islam, I. Ali, H.M. Khan, G. Mustafa, I. Ali, Ceram. Int**39**, 1539 (2013).
[26] F.N.A. Freire, M.R.P. Santos, F.M.M. Pereira, R.S.T.M. Sohn, J.S. Almeida, A.M.Medeiros, E.O. Sancho, M.M. Costa, A.S.B. Sombra, J. Mater. Sci.: Mater.Electron**20**, 149 (2009).
[27] IrshadAli , M.U. Islam , Muhammad Naeem Ashiq , M. Asif Iqbal, Hasan M. Khan , G. Murtaza, Journal of Magnetism and Magnetic Materials **362**, 115 (2014).
[28] A.V. Ramana Reddy, G. Ranga Mohan, B.S. Boyanov, D. Ravinder, Mater. Lett **39**, 153(1999).
[29] K. Vijaya Kumar, D.Ravinder, Int. J. Inorg. Mater**3**, 661 (2001).
[30] D. Ravinder, A.V. Ramana Reddy, Mater. Lett **38**,265 (1999).
[31] D. Ravinder, Mater. Lett 43,129 (2000).
[32] S. Sindhu, M.R. Anantharaman, B.P. Thampi, K.A. Malini, P. Kurian, Bull. Mater.Sci. **25**, 599(2002).
[33] J. Habasaki, K.L. Ngai, J. Non-Cryst. Solids 352, 5170 (2006).
[34] J.A.D. Guillén, M.R.D. Guillén, K.P. Padmasree, A.F. Fuentes, J. Santamaría,León, Solid State Ion**179**,2160 (2008).
[35] K.L. Ngai, C. León, Solid State Ion**125**,81(1999).
[36] S. Dutta, R.N.P. Choudhary, P.K. Sinha, Phys. Status Solidi A **202**,1172(2005).
[37] A.M. Abdeen, O.M. Hemeda, E.E. Assem, M.M. El-Sehly, J. Magn. Magn. Mater **238**,75(2002).
[38] E. Barsoukov, J.R. Mac Donald (Eds.), Impedance Spectroscopy Theory, Experi-ment, and Applications, Will-Interscience, second edn, John Wiley &Sons, Inc.,(2005).
[39] H. Anwar, A. Maqsood, J. Magn. Magn. Mater**333**,46(2013).
[40] M.A. Dar, K.M. Batoo, V. Verma, W.A. Siddiqui, R.K. Kotnala, J. Alloys Compd **493**, 553 (2010).
[41] Y. Bai, J. Zhou, Z. Gui, L. Li, J. Magn. Magn.Mater.**278**, 208 (2004).
[42] M.G. Chourashiya, J.Y. Patil, S.H. Pawar, L.D. Jadhav, Mater. Chem. Phys. **109**,39(2008).
[43] H.I. Hsiang, P.W. Cheng, F.S. Yen, Ceram. Int**38**,4915 (2012).